10326 *Inorg. Chem.* **2009**, *48*, 10326–10329
DOI: 10.1021/ic9014724

Inorganic Chemistry
Article

Biomineralization and Superhydrophobicity of $BaCO_3$ Complex Nanostructures

Shuisheng Wu,[†,‡] Huaqiang Cao,[*,†] Shuangfeng Yin,[*,‡] Xinrong Zhang,[†] and Victoria Chernow[§]

[†]*Department of Chemistry, Tsinghua University, Beijing, 100084, P.R. China,* [‡]*Department of Chemistry, Hunan University, Changsha, 410082, P. R. China, and* [§]*Department of Chemistry and Chemical Biology, Harvard University, Cambridge, Massachusetts 02138*

Received July 24, 2009

In this paper, we report on biomineralization of $BaCO_3$ hierarchical architectures with self-cleaning ability. The phase structures of the obtained samples were characterized by X-ray diffraction (XRD). All of these complex nanostructures, including dendrite-like nanostructures, dumbbell-like nanostructures, and spherical nanostructures of $BaCO_3$, were obtained by tuning the experimental parameters, such as the concentration of glucosan and Ba^{2+} cations. The morphology and structures were studied by scanning electron microscopy (SEM), transmission electron microscopy (TEM), high resolution TEM (HRTEM), and Fourier transform infrared (FT-IR) spectrum. The formation of dendrite-like, dumbbell-like, and spherical complex nanostructures can be explained by a rod−dumbbell−sphere (RDS) self-assembly growth mechanism. To our knowledge, this is the first demonstration of the biomimetic synthesis of $BaCO_3$ hierarchical architectures which uniquely display the characteristic of superhydrophobicity. A water contact angle of >150° and sliding angle of 1° of the $BaCO_3$ hierarchical architectures can be adjusted, which opens up a wide range of new potential applications of bioinspired complex nanostructures in environmental chemistry.

1. Introduction

It is the fine supermolecular arrangements of inorganic molecules that comprise the novel nanomaterials we find in nature—such arrangements varying from tens to hundreds of molecules in size and forming multidimensional structures which, via interaction with other materials, reveal striking chemical and physical functionalities.[1] Natural nanomaterials, such as shells, bones, and teeth, have inspired scientists and engineers to create complex synthetic materials biomimetically—science using nature as a guide in assembling materials with distinguished functions. It is believed that pursuing bioinspired approaches in constructing materials is one of the most promising and challenging scientific and technological endeavors of the coming years.[2]

In the process of uncovering the novel properties of nanomaterials, recreating superhydrophobicity has shown itself to be a particular synthetic challenge, it being necessary for a material to have a water contact angle greater than 150° to be characterized as superhydrophic. It is well-known, however, that the nanostructured surface of the lotus leaf, which repels water, displays superhydrophobic characteristics, given the combined physically rough micro- and nanostructures on the surface of the leaf, resulting in what is known as the lotus effect. This has become a symbol for the environmentally friendly aspects of nanotechnology.[3] Inspired by the lotus leaf, material scientists are currently engaged in constructing similar rough surface textures on membranes to obtain superhydrophobic properties. Yuan and co-workers reported self-standing nanowire membranes that exhibited controlled wetting behavior ranging from superhydrophilic to superhydrophobic.[4] Dorrer and co-workers reported a process for the fabrication of nanorough silicon surfaces modified with polymer monolayers which obtained superhydrophilic to superhydrophobic surfaces.[5] Nakanishi and co-workers reported nanocarbon-based superhydrophobic surfaces created from fullerene-based hierarchical supermolecular assemblies.[6] Luo and co-workers reported a superhydrophobic coating surface fabricated by a conventional curing process.[7] Xia and co-workers reported a superhydrophobic surface generated by electrohydrodynamic techniques.[8] Jokinen and co-workers reported superhydrophobic silicon nanograss fabricated by using a maskless deep reactive ion etching process.[9] Zorba and

*Corresponding authors. E-mail: hqcao@mail.tsinghua.edu.cn (H.C.); sf_yin@hnu.cn (S.Y.).

(1) Hornyak, G. L.; Dutta, J.; Tibbals, H. F.; Rao, A. K. *Introduction to Nanoscience*; CRC Press: Boca Raton, 2008.
(2) Sanchez, C.; Arribart, H.; Madeleine, M.; Guille, G. *Nat. Mater.* **2005**, *4*, 277.
(3) Jones, R. *Nat. Nanotechnol.* **2007**, *2*, 71.
(4) Yuan, J.; Liu, X.; Akbulut, O.; Hu, J.; Suib, S. L.; Kong, J.; Stellacci, F. *Nat. Nanotechnol.* **2008**, *3*, 332.
(5) Dorrer, C.; Rühe, J. *Adv. Mater.* **2008**, *20*, 159.
(6) Nakanishi, T.; Michinobu, T.; Yoshida, K.; Shirahata, N.; Ariga, K.; Möhwald, H.; Kurth, D. G. *Adv. Mater.* **2008**, *20*, 443.
(7) Luo, Z.; Zhang, Z.; Hu, L.; Liu, W.; Guo, Z.; Zhang, H. *Adv. Mater.* **2008**, *20*, 970.
(8) Xia, F.; Jiang, L. *Adv. Mater.* **2008**, *20*, 2842.
(9) Jokinen, V.; Sainiemi, L.; Franssila, S. *Adv. Mater.* **2008**, *20*, 3453.

 Published on Web 09/28/2009

co-workers reported creating biomimetic artificial superhydrophobic silicon surfaces.[10] Zhu and co-workers reported manufacturing superhydrophobic rambutan-like hollow spheres of polyaniline.[11] Lee and co-workers reported biomimetic superhydrophobic surfaces fabricated on high-density polyethylene surfaces by heat- and pressure-driven imprinting methods using patterned anodic aluminum oxides as replication templates.[12] Generally speaking, the construction of natural biomaterials has been a long-standing subject of material science, which is a great challenge at the present time.

In this paper, we report on biomineralization of $BaCO_3$ hierarchical architectures with self-cleaning ability. To our knowledge, this is the first demonstration of the biomimetic synthesis of $BaCO_3$ hierarchical architectures which uniquely display the characteristic of superhydrophobicity.

2. Experimental Section

Synthesis. All of the chemicals were used without further purification. The synthesis of $BaCO_3$ crystals was carried out by the gas diffusion method as reported.[13] The synthesis was carried out in glass bottles with a volume of 10 mL, which were put in a closed desiccator. The desiccator was placed in an oven at 30 °C. In a typical case, 320 μL of 10 mM $BaCl_2$ aqueous solution was added to 8 mL of 4 g/L glucosan [$(C_6H_{10}O_5)_n$, analytical reagent, AR, M_w = 20000] solution with stirring for 15 min. Several pieces of glass substrates were put at the bottom of the bottle for collecting the crystals. Each bottle was then covered with Parafilm, which was punched with three needle holes, and placed in a desiccator. Three small weighing bottles (10 mL) with crushed ammonium carbonate were also covered with Parafilm, each of which was punched with three needle holes and placed at the bottom of the desiccators. After different mineralization times, the Parafilm was removed, and the precipitate on the glass substrates that laid on the bottom was rinsed with deionized water and ethanol and allowed to dry at room temperature.

Characterization. Crystals were collected and characterized by powder X-ray diffraction (XRD) on a Bruker D8 Advance diffractometer using Cu Kα radiation (λ = 1.5406 Å). The scanning electron microscopy (SEM) images were obtained by a KYKY-2000 instrument. Transmission electron microscopy (TEM) images were taken with a JEOL, JEM-1200 instrument, using an accelerating voltage of 120 kV. High-resolution transmission electron microscopy (HRTEM) images were taken on a JEOL JEM-2010F electron microscope, operating at 200 kV. Fourier transform infrared (FT-IR) spectra were obtained with a NICOLET 560 Fourier transform infrared spectrophotometer.

Water Contact Angle (CA) Measurement. CA measurement was carried out on water droplet (drop volume 8 μL) on an optical contact angle meter (Data physics Inc., OCA 20) at ambient temperature.

3. Results and Discussion

The phase structures of the obtained samples were characterized by XRD, as shown in Figure 1. All the diffraction peaks can be attributed to pure orthorhombic $BaCO_3$ (JCPDS 71-2394). The diffraction peak (111) is the strongest,

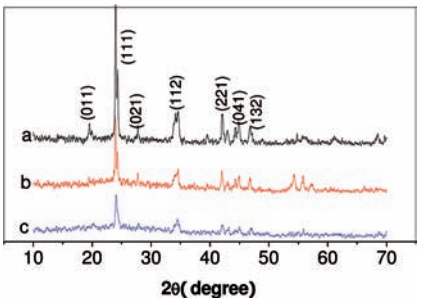

Figure 1. XRD patterns of as-synthesized samples: (a) obtained with the condition of Ba^{2+} concentration of 10 mM, glucosan concentration of 4 g L^{-1}, and reaction time 120 h denoted as **BCO-5**, (b) obtained with the condition of Ba^{2+} concentration of 40 mM, glucosan concentration of 4 g L^{-1}, and reaction time 120 h denoted as **BCO-7**, and (c) obtained with the condition of Ba^{2+} concentration of 10 mM, glucosan concentration of 16 g L^{-1}, and reaction time 120 h denoted as **BCO-9**.

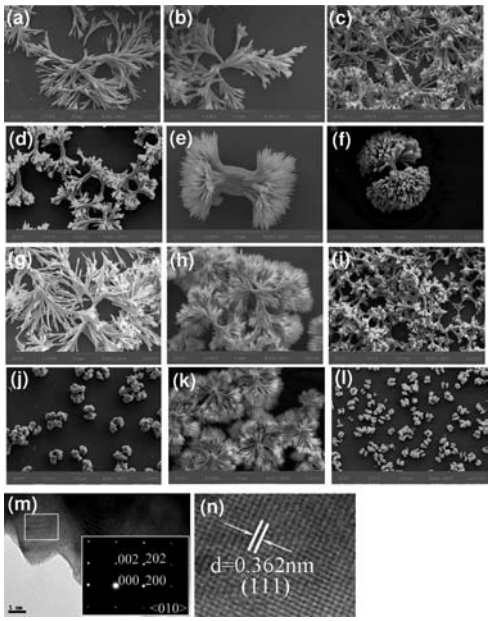

Figure 2. SEM images of products obtained with Ba^{2+} concentration of 10 mM and glucosan concentration of 4 g L^{-1} at the different reaction times: (a) 6 h (**BCO-1**), (b) 12 h (**BCO-2**), (c) 24 h (**BCO-3**), (d) 72 h (**BCO-4**), (e) 120 h (**BCO-5**), and (f) 240 h (**BCO-6**); SEM images of products obtained with glucosan concentration of 4 g L^{-1} and reaction time of 120 h at the different Ba^{2+} concentrations: (g) 40 mM (**BCO-7**) and (h) 20 mM (**BCO-8**); SEM images of products obtained with Ba^{2+} concentration of 10 mM and reaction time of 120 h at the different glucosan concentrations: (i) 16 g L^{-1} (**BCO-9**), (j) 8 g L^{-1} (**BCO-10**), (k) 1 g L^{-1} (**BCO-11**), and (l) 0.5 gL^{-1} (**BCO-12**); and (m and n) HRTEM images of **BCO-5**, inset in (m): the corresponding electron diffraction pattern (ED).

suggesting that the as-prepared $BaCO_3$ crystals were well oriented and grew mainly along the (111) face. This result was also maintained by SEM observation, which exhibited the rod morphology as a second order structure of complex $BaCO_3$ hierarchical architectures. No characteristic peaks from other impurities were found, suggesting that the as-synthesized samples were of high phase purity.

To investigate the growth process of biomimetic $BaCO_3$ nanostructures in our system, a series of contrast experiments were performed. Studied first was the effect of reaction time. Figure 2 show SEM images of the final $BaCO_3$ products synthesized in identical concentrations (Ba^{2+} concentration = 10 mM, glucosan concentration = 4 g L^{-1}) and identical

(10) Zorba, V.; Stratakis, E.; Barberoglou, M.; Spanakis, E.; Tzanetakis, P.; Anastasiadis, S. H.; Fotakis, C. *Adv. Mater.* **2008**, *20*, 4049.
(11) Zhu, Y.; Hu, D.; Wan, M.; Jiang, L.; Wei, Y. *Adv. Mater.* **2007**, *19*, 2092.
(12) Addadi, L.; Moradian, J.; Shay, E.; Maroudas, N. G.; Weiner, S. *Proc. Natl. Acad. Sci. U.S.A.* **1987**, *84*, 2732.
(13) Lee, Y.; Park, S.-H.; Kim, K.-B.; Lee, J.-K. *Adv. Mater.* **2007**, *19*, 2330.

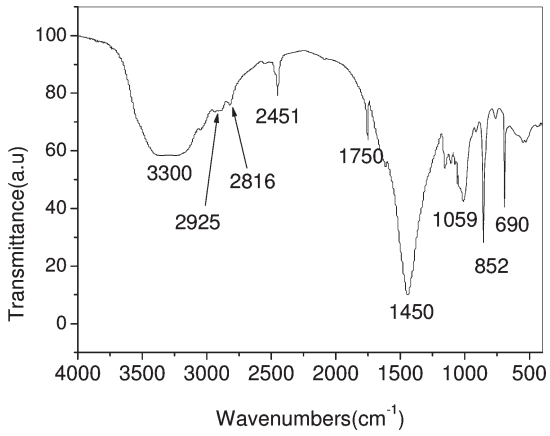

Figure 3. FT-IR spectrum of as **BCO-5**.

ratios of reactants, but for different reaction periods, that is, 6, 12, 24, 72, 120, and 240 h, these being denoted as **BCO-1**, **BCO-2**, **BCO-3**, **BCO-4**, **BCO-5**, and **BCO-6**, correspondingly. According to SEM observation, when the reaction time was within 72 h, the morphologies of the products were similar, appearing as dendrite-like structures (Figure 2a−d). When the reaction time was prolonged to 120 h, dumbbell-like nanostructures were obtained (Figure 2e), and going further, when the reaction time was prolonged to 240 h, spherical nanostructures were prepared (Figure 2f). All of these complex nanostructures, including dendrite-like nanostructures, dumbbell-like nanostructures, and spherical nanostructures, were composed of nanorods as second order compositions with diameters in the range of 400−600 nm.

We also investigated the effect of the concentration of Ba^{2+} on the morphology of the products. For this series of experiments, we decreased the concentration of Ba^{2+} from 40 to 20, to 10 mM with other conditions remaining constant—the concentration of glucosan remained at 4 g L^{-1} and the reaction time was kept at 120 h. The corresponding products are denoted as **BCO-7** (Figure 2g), **BCO-8** (Figure 2h), and **BCO-5** (Figure 2e), respectively. According to SEM observation, the morphologies changed from dendrite-like nanostructures to spherical nanostructures with decreasing concentrations of Ba^{2+}.

The effect of the concentration of glucosan on the morphology of the products was also investigated. After decreasing the concentration of glucosan from 16 to 8, 4, and 1 g L^{-1} with other reaction conditions remaining constant—the reaction time stayed at 120 h and Ba^{2+} concentration remained at 10 mM—we obtained dendrite-like $BaCO_3$ nanostructues (denoted as **BCO-9**) (Figure 2i), dumbbell-like $BaCO_3$ nanostructures (denoted as **BCO-10**) (Figure 2j), spherical $BaCO_3$ nanostructure (**BCO-5**) (Figure 2e), and spherical $BaCO_3$ nanostructures (denoted as **BCO-11**) (Figure 2k).

The structure of **BCO-5** was further studied by HRTEM, as shown in Figure 2m,n. The HRTEM images exhibit well-resolved 2D lattice fringes. Both the HRTEM and the ED pattern further confirmed the dumbbell-like nanostructures of **BCO-5** single-crystal in nature.

To identify the growth mechanism of $BaCO_3$ complex nanostructures, the sample was analyzed by FT-IR spectroscopy. A typical FT-IR spectrum of **BCO-5** is shown in Figure 3. The absorption bands at 690 and 852 cm^{-1} are attributed to the in-plane bending and out-of-plane bending modes of CO_3^{2-}, and the band at 1450 cm^{-1} is associated with asymmetric C−O stretching vibration,[14] while the weak band at 1059 cm^{-1} is attributed to the symmetric C−O stretching vibration.[15] The bands at 2816 and 2925 cm^{-1} can be attributed to the C−H stretching vibration of soluble glucosan molecules absorbed on the surface of $BaCO_3$ complex nanostructures.[16] The band at 3300 cm^{-1} can be attributed to ν(OH) stretching vibration due to hydrogen bonding. Usually, the O−H bands appear at a higher frequency of about 3630 cm^{-1} and have a sharp absorption peak.[17] However, the formation of hydrogen bonds resulted in a shift to lower wavenumbers, from 3500 to 2900 cm^{-1} and a broadening of O−H stretching bands of FT-IR data.[17] This absorption band at 3300 cm^{-1} indeed confirms the existence of hydrogen bonds in the complex $BaCO_3$ nanostructures, which contribute to the self-assembly of the superstructures.[18]

On the basis of SEM observation and FT-IR data, the growth mechanism for the generation of $BaCO_3$ complex nanostructures, as shown in Scheme 1, follows a rod−dumbbell−sphere (R-D-S) progression. The first stage is the nucleation process, that is, the initial reaction between Ba^{2+} and glucosan which generates the $BaCO_3$ nuclei. The second stage is the formation of $BaCO_3$ rods via orientation growth along with (111) face, as demonstrated by XRD and HRTEM data. The third stage involves the self-assembly of rods via hydrogen bonding (aggregation), leading to the formation of dumbbells, finally followed by the formation of spheres—thus illustrating the development of $BaCO_3$ nanoarchitectures.

All self-assembling systems are driven by some principle of energy minimization.[19] It is evident that the forces between molecules must be much weaker than the covalent bonds to hold molecules together for self-assembly to be possible in soft materials.[20] Compared with covalent bonds (about 500 kJ mol^{-1}), hydrogen bonds are energetically weaker (20 kJ mol^{-1}), a favorable circumstance for self-assembling superstructures not undergoing chemical reaction. Furthermore, hydrogen bonds are, in fact, strong enough to hold the superstructures together, given that the energy of a hydrogen bond is larger than the thermal energy (2.4 kJ mol^{-1}).[21] As demonstrated by the FT-IR data, it is hydrogen bonding between the rods of $BaCO_3$ that is responsible for holding the superstructure together. And the hydrogen bonds can be attributed to interaction of the −OH of glucosan molecules.

The surface of solids is important at all size scales. On the nanoscale level, however, surface phenomena prove to be particularly interesting. Indeed, it has been found that the lotus leaf displays superhydrophobic character, allowing water droplets to freely roll off the leaf into nearly perfect

(14) Chen, L.; Shen, Y.; Xie, A.; Zhu, J.; Wu, Z.; Yang, L. *Cryst. Res. Technol.* **2007**, *42*, 886.
(15) Lv, S.; Sheng, J.; Zhang, S.; Sun, W. *Mater. Res. Bull.* **2008**, *43*, 1099.
(16) Clayden, J.; Greeves, N.; Warren, S.; Wothers, P. *Organic Chemistry*; Oxford University Press: Oxford, U.K., 2001; p 69.
(17) Zhao, Z.; Zhou, X.; Zhang, W.; Zhao. W. *Instrumental Analysis*; Higher Education Press: Beijing, China, 1991; pp 87−88.
(18) Lee, Y. S. *Self-assembly and nanotechnology: a force balance approach*; John Wiley & Sons, Ltd.: Hoboken, NJ, 2008; pp 42−44.
(19) Pelesko, J. A. *Self-assembly: the science of things that put themselves together*; Chapman & Hall/CRC: 2007.
(20) Kelsall, R.; Hamley, I.; Geoghegan, M. *Nanoscale Science and Technology*; John Wiley & Sons Ltd.: West Sussex, U.K., 2005.
(21) Xiang, J.; Cao, H.; Warner, J. H.; Watt, A. A. R. *Cryst. Growth Des.* **2008**, *8*, 4583.

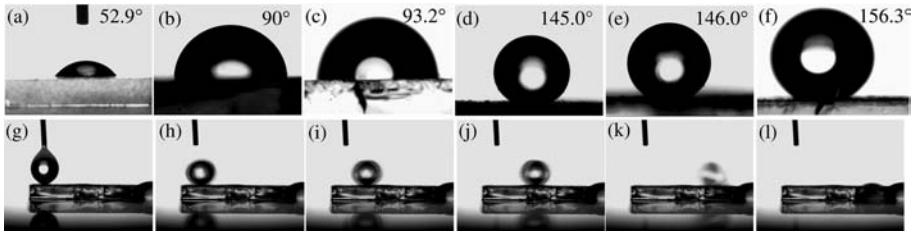

Figure 4. Water contact angle (CA) measurements of (a) glass, (b) glass coated with Au, then *n*-dodecanethiol molecules, (c) glass coated with Au, then 1*H*,1*H*,2*H*,2*H*-perfluorodecyltriethoxysilane molecules, (d) glass coated with $BaCO_3$ nanostructures 8 times, followed by gold layer and *n*-dodecanethiol, successively, (e) glass coated with $BaCO_3$ nanostructures 24 times, followed by gold layer and *n*-dodecanethiol, successively, (f) glass coated with $BaCO_3$ nanostructures 8 times, followed by gold layer and 1*H*,1*H*,2*H*,2*H*-perfluorodecyltriethoxysilane, successively; (g−l) corresponding sliding angle measurement of the glass coated with $BaCO_3$ nanostructures 8 times, followed by gold layer and 1*H*,1*H*,2*H*,2*H*-perfluorodecyltriethoxysilane.

Scheme 1. Complex $BaCO_3$ Rod−Dumbbell−Spheres (RDS) Growth Mechanism

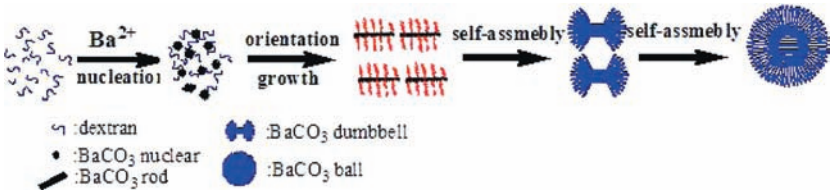

spheres, while allowing oil to selectively spread. This phenomenon called the lotus effect[1] can be attributed to the lotus leaf surface being composed of unique micro- and nanostructures. The ability of the nanostructured surface of the lotus leaf to repel water has become a symbol for the environmentally friendly qualities of nanotechnology.[3] Given the lotus effect and the general prevalence of nanostructures in natural materials, we were inspired to biomimetically synthesize complex nanoassemblies, like spherical $BaCO_3$, and study their superhydrophobicity by means of measuring CA. The CA is the angle formed by a liquid drop at the three-phase boundary where a liquid, gas, and solid intersect, and it is included between the tangent plane to the surface of the liquid and the tangent plane to the surface of the solid, at the point of intersection. Given this, the CA is a quantitative measure of the wetting of a solid by a liquid.[22]

As shown in Figure 4, the CA value of the glass surface was initially 55.6 ± 2.7° (Figure 4a showing the CA of 52.9°). The CA value changed to 90° after the glass surface was coated with a layer of gold, followed by treatment with *n*-dodecanethiol (Figure 4b). This value again changed to 93.2° after the glass surface was coated with a layer of gold, followed by treatment with 1*H*,1*H*,2*H*,2*H*-perfluorodecyltriethoxysilane-[$(C_2H_5O)_3Si(CH_2)_2C_8F_{17}$] (Figure 4c).

Comparatively, the CA values of the glass surface modified by coating with as-synthesized $BaCO_3$ nanostructures are shown in Figure 1d−f. The CA was 145.0° after coating the glass 8 times with $BaCO_3$ nanostructures, followed by treatment with a layer of gold and then *n*-dodecanethiol (Figure 4d); the CA was 146.0° after coating the glass with $BaCO_3$ nanostructures 24 times, followed by successive addition of gold layer and *n*-dodecanethiol (Figure 4e). That means the as-synthesized $BaCO_3$ nanostructures can indeed change the wettability of the glass; however, the effect of the modifying times of $BaCO_3$ nanostructures is limited. Also revealed is the fact that glass, when modified by as-synthesized $BaCO_3$ nanostructures and *n*-dodecanetionol, has a hydrophobic surface. However, the CA only reaches a superhydrophobic level of 156.3° [accompanying with sliding angle of 1°, Figure 4g−l and Supporting Information, Movie S1] after the glass coated with $BaCO_3$ nanostructures 8 times, followed by application of a gold layer and then $(C_2H_5O)_3Si(CH_2)_2C_8F_{17}$ (Figure 4f). Such results imply the real possibility of introducing large-scale industrial fabrication of superhydrophobic surfaces with novel self-cleaning and anticorrosion properties.[23]

In summary, we report the formation $BaCO_3$ complex nanostructures consisting of nanorods. The relationship between the reaction time, reactant concentrations, and morphology of $BaCO_3$ complex nanostructures is analyzed herein. The formation of dendrite-like, dumbbell-like, and spherical complex nanostructures can be explained by a rod−dumbbell−sphere (RDS) self-assembly growth mechanism. Additionally, the controlled wetting behavior and superhydrophobicity of the $BaCO_3$ complex nanostructures is demonstrated. Many other technical studies are expected to follow and will expound on the potential of complex nanostructures used in environmental protection applications. Bioinspired approaches to constructing nanomaterials with novel self-cleaning properties are certainly some of the most interesting scientific and technological challenges of the near future. Indeed, the creation of biofriendly and biomimetic materials is without doubt at the frontier of all scientific fields, influencing everything from chemistry and material science to biology and, of course, nanotechnology.

Acknowledgment. The authors gratefully thank financial support from the National Natural Science Foundation of China (No. 20671056 and 20535020), the Innovation Method Fund of China (No. 20081885189), and the National High Technology Research and Development Program of China (No. 2009AA03Z321).

Supporting Information Available: Movie of the sliding angle measurement of as-synthesized $BaCO_3$ nanostructures. This material is available free of charge via the Internet at http://pubs.acs.org.

(22) Erbil, H. Y. *Surface Chemistry of Solid and Liquid Interfaces*; Blackwell Publishing Ltd.: Oxford, U.K., 2006.

(23) Wang, S.; Feng, L.; Jiang, L. *Adv. Mater.* **2006**, *18*, 767.